HHS Public Access

Author manuscript

Cancer Res. Author manuscript; available in PMC 2020 May 01.

Published in final edited form as:

Cancer Res. 2019 May 01; 79(9): 2327–2338. doi:10.1158/0008-5472.CAN-18-1785.

Selective EGLN Inhibition Enables Ablative Radiotherapy and Improves Survival in Unresectable Pancreatic Cancer

Tara N. Fujimoto[1,*], **Lauren E. Colbert**[2,*], **Yanqing Huang**[1,*], **Jessica M. Molkentine**[1], **Amit Deorukhkar**[1], **Laura Baseler**[3], **Marimar de la Cruz Bonilla**[1], **Meifang Yu**[1], **Daniel Lin**[1], **Sonal Gupta**[4,5], **Peter K. Cabeceiras**[1], **Charles V. Kingsley**[6], **Ramesh C. Tailor**[7], **Gabriel O. Sawakuchi**[7], **Eugene J. Koay**[2], **Helen Piwnica-Worms**[1], **Anirban Maitra**[4,5], **Cullen M. Taniguchi**[1,2,†]

[1]Department of Experimental Radiation Oncology, The University of Texas MD Anderson Cancer Center, Houston, TX 77030

[2]Department of Radiation Oncology, The University of Texas MD Anderson Cancer Center, Houston, TX 77030

[3]Dept. of Veterinary Medicine & Surgery, UT MD Anderson Cancer Center, Houston, TX 77030

[4]Dept. of Pathology, UT MD Anderson Cancer Center, Houston, TX 77030

[5]Dept. of Translational Molecular Pathology, UT MD Anderson Cancer Center, Houston, TX 77030

[6]Dept. of Imaging Physics, UT MD Anderson Cancer Center, Houston, TX 77030

[7]Department of Radiation Physics, UT MD Anderson Cancer Center, Houston, TX 77030

Abstract

When pancreatic cancer cannot be removed surgically, patients frequently experience morbidity and death from progression of their primary tumor. Radiation therapy cannot yet substitute for an operation because radiation causes fatal bleeding and ulceration of the nearby stomach and intestines before achieving tumor control. There are no FDA-approved medications that prevent or reduce radiation-induced gastrointestinal injury. Here, we overcome this fundamental problem of anatomy and biology with the use of the oral EGLN inhibitor FG-4592, which selectively protects the intestinal tract from radiation toxicity without protecting tumors. A total of 70 KPC mice with autochthonous pancreatic tumors received oral FG-4592 or vehicle control +/- ablative radiation therapy (RT) to a cumulative 75Gy administered in 15 daily fractions to a limited tumor field. Although ablative RT reduced complications from local tumor progression, fatal gastrointestinal bleeding was observed in 56% of mice that received high-dose RT with vehicle control. On the other hand, radiation-induced bleeding was completely ameliorated in mice that received high-dose RT with FG-4592 (0% bleeding, $P<.0001$ compared to vehicle). Furthermore, FG-4592 reduced epithelial apoptosis by two-fold ($P=0.002$) and increased intestinal microvessel density by 80% compared to vehicle controls. EGLN inhibition did not stimulate cancer growth, as treatment

[†]To whom correspondence should be addressed: Cullen M. Taniguchi, MD PhD, The University of Texas MD Anderson Cancer Center, Division of Radiation Oncology, 1515 Holcombe Blvd, Unit 1050, Houston, TX 77030-4000, ctaniguchi@mdanderson.org.
[*]These authors contributed equally

Disclosures: The authors declare no conflicts of interest in this manuscript.

with FG-4592 alone, or overexpression of HIF2 within KPC tumors independently improved survival. Thus, we provide a proof-of-concept for the selective protection of the intestinal tract by the EGLN inhibition to enable ablative doses of cytotoxic therapy in unresectable pancreatic cancer by reducing untoward morbidity and death from radiation-induced gastrointestinal bleeding.

Keywords

Pancreatic cancer; Radiation Therapy; EGLN, Radioprotection; HIF; hypoxia; locally advanced pancreatic cancer; PDAC

Introduction

Pancreatic cancer is a deadly disease that is now projected to be the second leading cause of cancer-related deaths by 2030 (1). Surgical excision of the primary pancreatic tumor is preferred when possible, but most patients present with unresectable disease (locally advanced + metastatic), leaving very few therapeutic options once chemotherapy is completed (2). Definitive treatment for pancreatic cancer is extremely important because progression of the primary tumor causes morbidity and mortality by invading into nearby organs and blood vessels, and is the primary cause of death in at least 30% of all pancreatic cancer patients (3).

When surgery is not an option, radiation therapy (RT) is the only modality proven to provide local control. The efficacy of conventional RT against pancreatic cancer is limited, since the radiation dose is modest due to potential radiotoxicity to the nearby stomach and intestines (4). The advent of conformal hypofractionated radiation treatments such as stereotactic body radiotherapy (SBRT) or image-guided IMRT (5) has overcome many of these problems (6), but unfortunately, radiation toxicity is still unavoidable since pancreatic tumors often invade into or abut the gastrointestinal tract, which is extremely sensitive to radiation damage (7).

The most common gastrointestinal toxicities from ablative radiation to the pancreas relates to reduced gastrointestinal absorptive functions, such as diarrhea and and dehydration. These can be treated with supportive management and patients can often expect to recover. Perhaps the most worrisome side effect is gastrointestinal bleeding from a radiation–induced ulcer, which is a rare, but potentially lethal toxicity that can occur when giving ablative doses of radiation for pancreatic cancer (8,9). Thus, treatment-related gastrointestinal (GI) toxicity may be the single greatest barrier to improving treatment responses for unresectable pancreatic cancer, but there are no known medications that can selectively protect the stomach and intestines from these side effects.

The EGLN family of α-ketoglutarate-dependent prolyl hydroxylases regulate the cellular response to hypoxia by directing the destruction of the hypoxia-inducible factor (HIF) family of transcription factors under normal oxygen tension (10). When EGLN proteins are inhibited genetically or pharmacologically, HIF is stabilized in normoxic tissues, which allows exploitation of the potentially therapeutic benefits of this pathway. We and others have previously demonstrated that pan-inhibition of all three mammalian isoforms of EGLN

mitigates and protects animals from otherwise lethal doses of gastrointestinal radiation (11–13). These studies used the drug dimethyloxallylglycine (DMOG), which is an efficacious EGLN inhibitor, but has undesirable pharmacokinetics for clinical use (14).

EGLN inhibitors have recently completed Phase III trials for a non-oncologic indication (15) and we reasoned that if this class of drugs was also effective at reducing radiation toxicity in a clinically relevant setting that they could be rapidly repurposed to treat pancreatic cancer. Here, we demonstrate that FG-4592, a clinically and pharmacologically relevant pan-EGLN inhibitor (16), significantly reduces gastrointestinal toxicity from ablative radiation treatments. Radioprotection does not affect tumor growth but increases the lifespan of treated mice by reducing both tumor-related and RT-related morbidity, which provides a proof-of-concept for this approach.

Materials and Methods

Animal Experiments

Mouse experiments were approved by the University of Texas MD Anderson Institutional Animal Care and Use Committee (IACUC) and were executed in accordance with the NIH guidelines for use and care of live animals under the protocol number 00001252-RN01. Mice were exposed to 12-hour light/dark cycles and given free access to standard rodent chow (Prolab Isopro RMH 3000 Irradiated Feed) and sterilized water. C57BL/6J mice were obtained from Jackson Laboratories. *Kras*$^{LSL/+}$ and *Trp53*$^{FL/FL}$;*Ptf1a*$^{Cre/+}$ animals were backcrossed to a pure C57BL/6 background over ten generations and then bred to each other to produce the desired *Kras*$^{LSL/+}$;*Trp53*$^{FL/+}$;*Ptf1a*$^{Cre/+}$ animals with 1:4 Mendelian frequency. Genotyping was performed as described previously (17). Littermate controls were used in all experiments and also co-housed with littermates before and after radiation. Single housing was avoided whenever possible.

Diagnosis, Small Animal Ultrasound and Tumor Measurements

KPC mice with a heterozygous *Trp53* deletion typically presented at 16–30 weeks of age. Thus, at 16 weeks of age, mice were subjected to weekly screening for tumors by brief exposure to inhaled anesthesia followed by abdominal palpation. Tumors can be palpated from as small as 3mm. Mice with any suspicious lesion on palpation were subjected to ultrasound. Briefly, mice were subjected to 2% isoflurane for anesthesia, then shaved with veterinary clippers and briefly treated with epilation cream. Animals were then placed supine onto a warmed ultrasound bed of a Vevo 2100 system (FujiFilm VisualSonics, Toronto, ON, Canada). A 30MHz transducer was used to acquire B-MODE long and short axis acquisitions. In addition, a 3D acquisition was also acquired and rendered to better estimate the tumor volume. Tumor measurements were made weekly and throughout treatment until death.

Small Animal Irradiation and Dosimetry

Radiation treatments were administered for 5 consecutive days per week, typically Monday-Friday, followed by a 2-day break (typically Saturday and Sunday) for a total of 15 fractions.

Thus a minimum treatment of 15 fractions would take placed over 19 calendar days. Prior to irradiation, anesthesia was induced with 2–3% isoflurane gas mixed with 1L oxygen, then maintained at 1–2% isoflurane mixed also with 1L oxygen. The radiation dose was delivered with the PXi X-RAD 225Cx image-guided irradiator from Precision X-Ray, Inc (North Branford, CT). The irradiator combines high-accuracy cone-beam CT (CBCT) imaging (resolution 0.2 mm) and orthovoltage (225 kVp) dose delivery. Each mouse was imaged using the PXi XRAD 225Cx irradiator fitted with a circular 15mm collimator. A cone beam CT prior to irradiation was performed to align the isocenter prior to treatment. The cranial edge of a 15mm circular field was aligned with the curve of the diaphragm on a coronal scout film and the isocenter was then placed in the mid-abdomen over the tumor, which was defined by ultrasound. Mice received a total of 5Gy per fraction, which was treated by equally weighted AP/PA fields (2.5Gy AP and 2.5Gy PA). Imaging dose from cone-Beam CT was negligible (<1 cGy/min). The dose output of the PXi XRAD 225Cx irradiator was measured with a 0.6cc Farmer chamber FC65G (SN 2247) in the reference geometry (10cm × 10cm) at its isocenter (32.4 cm). The Farmer chamber's Calibration-Factor (Nk) was provided by the MD Anderson's Accredited Dosimetry Calibration Laboratory, and is traceable to NIST. Other dosimetry parameters for the Applicators were measured with combination of ion-chamber and film (EBT2, EBT3). The unit's dose-output constancy was checked prior setting-up animal for irradiation.

FG-4592 administration

The EGLN inhibitor, FG-4592 (Cayman Chemical, #15294, Ann Arbor, MI) was administered by oral gavage at a dose of 40mg/kg in 0.5 (w/v)% sterilized methyl cellulose 400 solution (Wako Pure Chemical Industries, Ltd; 133–17815, Richmond, VA). The initial dose of vehicle or FG-4592 treatment was typically administered 5 days after diagnosis, which was timed to coincide with radiation treatments, if the mice were assigned to receive them. FG-4592 or vehicle control was initiated the day prior to starting radiation and then 6 hours prior to radiation on any day of radiation treatment. Drug or vehicle dosing continued 4x/week during treatment, which were typically Monday, Wednesday, Friday and Sunday. The treatment was considered complete after 13 total treatments were administered over 3 weeks. On days when mice received both FG-4592 and radiation, FG-4592 was given 3 hours prior to radiation.

Metabolic Cage Experiments

Eight week old male C57BL/6J mice were treated with a 15 fraction course of upper abdominal radiation with FG-4592 or vehicle control for radioperotection as described above. Mice were acclimated to the metabolic cages (Braintree Scientific, Braintree, MA) for one week prior to radiation. Body weight, food, and water consumption as well as urine & fecal output were monitored daily for the entire study period, which includes radiation on weekdays and treatment breaks on weekends. All treatments were started on a Monday. Data are plotted from the first dose of radiation. Area under the curve was estimated by the trapezoid method (18) and plotted with units appropriate to each parent graph.

Cell Culture and Cell Lines

The KPC cell line was a kind gift from Dr. Anirban Maitra, and was derived from a spontaneous tumor from a female *KrasG12D*$^{LSL/+}$*; Trp53 R172H; Pdx1-Cre (KPC)* mouse, which was backcrossed over 10 generations to C57BL/6. The HIF2 overexpressing cell lines (TetOn-HIF2 KPC) were generated using this parental KPC line. All KPC cell lines were maintained in RPMI 1640 (Sigma Aldrich, St. Louis, MO) and were supplemented with 1% GlutaMAX™, 1% sodium pyruvate, and recombinant insulin (all from Life Technologies, Grand Island, NY). Media were supplemented with 10% regular fetal bovine serum (Heat-Inactivated; Sigma Aldrich) for KPC cell line except for HIF2 overexpressing clones (TetOn-HIF2), which were maintained in media containing 10% Tet-System approved fetal bovine serum (Takara Bio USA, Mountain View, CA). All cell lines were authenticated by short tandem repeat (STR) profiling, which establishes genetic profile using 31 species-specific STR markers and checks for interspecies contamination (human/ mouse/ rat/ monkey/ Chinese hamster), and were confirmed to be free of Mycoplasma (CellCheck Mouse Plus testing, IDEXX Laboratories, Inc., Columbia, MO; Case # 7564–2018).

For the Tet-On HIF2 cell lines, the human HIF2α (*EPAS1*) coding sequence was synthesized (Genscript, Piscataway, NJ) with an N-terminal 3xFlag sequence and mutations at P405A, P564A and N847A, to render the protein stable and transcriptionally active during normoxia (19). This mutant construct was subcloned into the pLVX TetOne-Puro vector (Clontech, Mountain View, CA), and lentiviruses were generated using the manufacturer's protocol. KPC cells were infected by spinfection at 1200g for 45 min then returned to the incubator. Puromycin selection was initiated 24h after spinfection, and completed when all control infected KPC cells were dead. Single clones were then selected and screened for doxycycline-inducible expression of HIF2 by western blot.

Orthotopic Injection Procedure

TetOn-HIF2 KPC cells were resuspended in ice-cold PBS and mixed with chilled Matrigel in a 1:1 ratio. Mice were anesthetized with 2% isoflurane and supported with artificial eye drops and a prophylactic dose of 0.1 mg/kg extended release buprenorphine given subcutaneously. Mice were placed in the right lateral decubitus position on a heating pad and fur was shaved and wiped with a 10% povidone iodine solution and 70% ethanol. Through a 1.5 cm incision with sterile surgical instruments, the spleen was visualized and removed from the abdominal cavity to expose the underlying tail of the pancreas. The 1:1 mixture of tumor:Matrigel was injected into the pancreatic parenchyma and directly observed until the wheal solidified. The organs were returned to their approximate anatomic position and the abdomen was closed with absorbable 6–0 sutures and sterile surgical staples. The mice were directly observed as they recovered from their operation on a heating pad. The next day after the procedure, mice were started on water with 200 μg/mL doxycycline or PBS, and changed on a weekly basis or earlier if required. Tumors were monitored 2x/week with ultrasound.

Immunoblotting

Total protein was extracted by homogenizing tissues in a proprietary tissue extraction buffer (T-PER; ThermoFisher Scientific, Waltham, MA, 78519), supplemented with protease and phosphatase inhibitor cocktails (Roche Applied Science, Indianapolis, IN) and denatured with 4x Laemmli sample buffer (Bio-Rad, Hercules, CA, 161–0747) and fractionated by SDS-PAGE. The proteins were electro-transferred to nitrocellulose membranes using the Trans-blot Turbo system (Bio-Rad), then blocked with TBS-T +5% skim milk powder. The blots were probed with primary antibodies diluted in Superblock T20 (ThermoFisher Scientific, Waltham, MA, 37536). HIF-1α (Novus Biologicals, Littleton, CO, NB100–105) was used at 1:500, and HIF-2α/ EPAS1 Novus Biologicals, NB100–122) was used at 1:1000 while β-actin (Cell Signaling Technology, Danvers, MA, #4970) was used at 1:1000. The blots were developed using Clarity™ Western ECL substrate (Bio-Rad). All protein expression data were quantified by Chemi-Doc XRS+ system (Bio-Rad).

Mouse Histology, Cause of Death, and Necropsy

Mice were subjected to necropsy when they met any euthanasia criteria. Mice were euthanized by CO2 followed by exsanguination via cardiac puncture. Causes of death were assigned after a complete necropsy, but were usually obvious on the initial examination, such as intestinal bleeding, duodenal or gastric outlet obstruction, large central lung metastases, or diffuse carcinomatosis. For necropsies, tissues were collected and fixed in 10% neutral-buffered formalin. Bones were decalcified in 10% formic acid (Fisher Scientific). Fixed tissues were embedded in paraffin; and tissue sections 4 microns in thickness were placed on slide and stained with hematoxylin and eosin (H&E) and analyzed by a veterinary pathologist (LB).

Histopathology and Immunohistochemistry

Histopathological analyses of longitudinal sections were carried out as published previously (20). Briefly, intestines were flushed with cold PBS then 10% neutral buffered formalin. Longitudinal sections were then pinned flat in a wax box and kept in neutral buffered formalin overnight. These fixed intestinal sections were then embedded in ddH2O containing 2% (w/v) agar then were paraffin-embedded. Five micron slices were then placed onto slides and stained with H&E. Images were acquired using Nikon Eclipse Ni-E microscope, with 10x objective, a Nikon Ds-Fi2 camera, and NIS-Elements Advanced Research software was used to stitch multiple fields together (Nikon USA, Melville, NY).

For immunohistochemistry analysis, slides were dewaxed and rehydrated and sodium citrate used for antigen retrieval. Slides were rinsed and blocked with 2.5% normal goat serum for 1 hour then incubated with MECA-32 antibody (1:100, Novus, NB100–77668SS) overnight at 4°C. Following the primary antibody, slides were incubated with peroxidase-conjugated secondary antibody and developed with DAB substrate kit (all from vector laboratories). Slides were counterstained with hematoxylin, dehydrated, and mounted with Permount.

TUNEL assay was performed with In Situ Cell Death Detection Kit, TMR red, (Sigma Aldrich). Tissue sections were dewaxed and rehydrated according to standard protocol

before incubating at 37°C for 30 mins with 15μg/ml ProteinaseK. Slides were rinsed twice with PBS and incubated with TUNEL reaction mixture at 37°C in the dark for 1 hour. Slides were rinsed twice with PBS and mounted with DAPI mounting medium before confocal imaging with an Olympus FV500 laser scanning confocal microscope (Olympus USA, Center Valley, PA).

Quantitative Reverse Transcription PCR (qPCR) Analysis

Tissue RNA was extracted with RNeasy Mini Kit (QIAGEN, Germantown, MD) and reverse transcription was performed using the QuantiTect ReverseTranscription Kit per the manufacturer's protocol (QIAGEN). qPCR was carried out using SYBR Green master mix on a CX384 real-time PCR machine (Bio-Rad). Primers for murine *Vegf* were designed across exon boundaries with an estimated melting point of 60°C and then synthesized by IDT Technologies (Skokie, IL) with the following sequences: *Vegf* Forward: TTCGTCCAACTTCTGGGCTC and *Vegf* Reverse: CTGGGACCACTTGGCATGG.

Statistical Methods

Descriptive statistics were generated for all mice. Mice who received >65Gy RT were considered as receiving full dose RT and completing treatment. Mice who received <=65Gy RT were considered as having received low dose RT. All mice were included in survival analyses. For mice who underwent necropsy, only mice who received full dose RT were included in comparisons. Sensitivity analyses were performed to demonstrate that exclusion of low-dose RT mice had no impact. Pathologic characteristics were compared using chi square of Fisher's exact test, where appropriate. Kaplan-Meier survival curves were generated for all mice, grouped by treatment group. All mice were censored when there were less than 1 mice in all treatment groups (after 50 days). Log-rank test was used to compare overall trends and also for individual stratum comparisons. JMP SAS version 12.0 was used for statistical analyses.

Results

The EGLN inhibitor FG-4592 Significantly Reduces Gastrointestinal Toxicity from Fractionated Radiation

To test whether FG-4592 stabilizes intestinal HIF expression, the drug or vehicle control was administered orally to C57BL/6J mice. We found low baseline levels of HIF1 and HIF2 in the duodenum and jejunum in control mice (Figure 1A), confirming low levels of hypoxia in this normal tissue. The administration of FG-4592, however, stabilized HIF levels by ten-fold (Figure 1A, with raw blots in Fig S1).

Current preclinical models for therapeutic radiation are often derived from models of catastrophic radiation to large fields, such as a single, lethal exposure to the whole body or whole abdomen of an animal (21). These radiation fields are not clinically relevant because the doses are subtherapeutic (22) and cause excessive radiation-induced toxicity (21,23). To mimic the fields, doses, and potential side effects of ablative radiation treatments used in the clinic (24), we treated wild-type, C57BL/6J mice with a circular 15mm subdiaphragmatic

radiation field, which contains the pancreas, duodenum, and portions of the jejunum, stomach, and liver (Figure 1B). Initial studies using a dose of 67.5Gy in 15 daily fractions (BED_{10}=97.8Gy, EQD2=81.6Gy), showed no death at 10 days (Figure S2). We increased the dose to 75Gy in 15 daily fractions (BED_{10}=112.5Gy, EQD2=93.8Gy) to this same focused treatment area, with pharmacological radioprotection afforded by either oral FG-4592 or a vehicle control. That modest increase in the dose was sufficient to cause 100% of the control mice to die by 10 days after radiation, which is consistent with death from GI complications. Strikingly, the administration of FG-4592 resulted in 100% survival of mice up to 30 days after RT (Figure 1C, log-rank $P<.0001$). Necropsies of the control mice revealed gastrointestinal bleeding in the form of congealed, digested blood in the intestinal tract of nearly all dead mice (9/10), which was consistent with observed clinical toxicity (8) (Figure 1D).

FG-4592 Does Not Enhance HIF Expression in Tumors

A radioprotector should preferentially shield normal tissues without any protection of cancer cells to have clinical utility. We have previously shown that HIF2 radioprotects the intestines (11) but were concerned with the theoretical risk that FG-4592 could also stabilize HIF levels in pancreatic tumors, thereby protecting cancer cells along with the intestinal crypts from radiation damage. To test this possibility, we bred KPC mice genetically characterized by a conditionally activated *Kras* allele (G12D) and a heterozygous *Trp53* loss-of-function allele, driven by a pancreas-specific Cre (*Ptf1a*-Cre) (25). Western blot analysis for HIF1 and HIF2 on lysates derived from these autochthonous pancreatic tumors showed robust expression of each HIF isoform in tumors treated with vehicle alone (Figure 2A, quantified in Figure 2B and raw blots in Figure S1), suggesting a high baseline level of hypoxia in these tumors, which has been reported previously (26). Interestingly, FG-4592 did not further increase the expression of either HIF1 or HIF2 compared to vehicle (Figure 2A and quantified in Figure 2B), suggesting that HIF expression in pancreatic tumors might already be maximized, even with the addition EGLN inhibition.

Intratumoral Expression of Stabilized HIF2α Does Not Promote Tumor Growth

To further ensure that HIF stabilization did not enhance the growth of pancreatic cancer, we created KPC cells with a nondegradable form of HIF2 whose expression is controlled in a doxycycline-dependent fashion (TetOn-HIF2 KPC). TetOn-HIF2 KPC cells syngeneic to C57BL/6 were implanted orthotopically into the pancreata of recipient BL/6 mice and HIF2 expression was activated with doxycycline or control drinking water. Immunoblot analysis revealed higher levels of stabilized HIF2 in tumors (Figure 2C), but this did not enhance pancreatic cancer progression, and instead surprisingly suppressed tumor growth (Figure 2D and 2E) and improved survival (Figure 2F), which is consistent with other published studies (27).

Ablative Radiation Therapy with EGLN Inhibition Improves Survival in KPC Mice

We then designed a preclinical trial to determine if FG-4592 would radioprotect the intestines sufficiently to enable ablative doses of radiation therapy. Towards this end, we backcrossed KPC mice over 10 generations to a C57BL/6 genetic background to reduce potential variability in normal tissue radiation responses that often occurs in mixed

backgrounds (28). Importantly, KPC mice with *Trp53* loss of heteozygosity present with predominantly locally advanced disease (29), which affords a window for intensive local treatment with radiation, both with and without radioprotection.

The experimental scheme is shown in Figure 3A. KPC mice were screened for pancreatic tumors by weekly ultrasounds, and when a tumor was identified, mice were sequentially assigned to receive one of four possible treatments: vehicle only (VEH), FG-4592 only (FG), RT concurrent with vehicle (RT+VEH), or RT concurrent with FG-4592 (RT+FG). Mice were treated on a rolling basis and the total time from diagnosis to treatment end was approximately three weeks. Animals assigned to arms with radiation were prescribed a total of 75Gy given in 15 daily fractions (5), using the fields in Figure 1B. Mice that received >65Gy or higher were considered to have received high-dose RT, while those who received ≤65Gy were considered to received low-dose RT.

Seventy mice with palpable, spontaneous pancreatic tumors were evaluated and underwent treatment. Their characteristics and outcomes are described in Table S1. A total of 39 mice were assigned to an arm without radiation, which included vehicle treatment alone (N=28) or oral FG-4592 alone (N=11). Thirty-one mice were assigned to high-dose fractionated radiation, with a vehicle (N=13) or oral FG-4592 (N=18). The tumor-bearing animals were similar between treatment groups in terms of in age (Figure S3A), weight (Figure S3B), and tumor volume (Figure S3C), with no statistical differences between the groups. There were no statistical differences in the ability to complete treatment between these groups.

Cohorts of mice that received focal radiation therapy (Any-RT, defined as RT+VEH or RT +FG groups) to pancreatic tumors showed improved overall survival (Figure 3B) compared to mice that did not receive radiation as a component of their treatment (No-RT, defined as VEH or FG groups). The median overall survival of the No-RT groups was 15 days compared to 26.5 days for the mice that received RT ($P = 0.006$). The median overall survival was compared amongst the treatment groups and was highest (Figure 3C; overall $P < .0001$) for mice that received RT with FG-4592 for radioprotection (43 days, [95% CI 39–47]) versus RT with vehicle (36 days, [95% CI 10–62]), FG alone (29 days, [95% CI 21–37]), or vehicle alone (9 days, [95% CI 5–13]). The primary comparison of mice that received high-dose RT with FG-4592 for radioprotection versus high-dose RT with vehicle was also significant. Interestingly, treatment with FG alone also improved survival compared to vehicle controls. These data further underscore the fact that EGLN inhibition and subsequent HIF2 expression do not promote pancreatic cancer growth, and may actually suppress it.

Ablative Radiation Reduces Symptoms of Local Progression

During treatment, mice were monitored twice daily and any animals that met criteria for euthanasia were sacrificed and subjected to a blinded necropsy under the supervision of a veterinary pathologist, who also assigned causes of death. Mice were euthanized when their tumors met size criteria, were moribund or exhibited signs of distress. At the time of euthanasia, a full necropsy was performed and a likely cause of death was assigned by a verterninary pathologist (LB, Table S2) based on the the most compelling pathologic lesion. For instance, if a mouse had a large obstructive tumor that caused bleeding with a few metastatic lesions, the death was attributed to local progression. The most common reasons

for euthanasia from local progression was tumor invading the stomach, intestines, liver or kidneys causing the mouse to become moribund (Table S2). When metastases were attributed as the cause of death, there was usually overwhelming carcinomatosis or embolic lung lesions (Table S2).

Morbidity caused by local tumor invasion was usually visible at necropsy, as depicted in Figure 3D. The use of ablative RT reduced death attributable to local tumor progression, as only 17% (3/17) of mice that received ablative doses of RT >65Gy exhibited morbidity and death from local obstruction (Figure 3E; $P<.0001$). In contrast, local obstructive symptoms were associated with 73% (27/37) of deaths in mice that did not receive RT as part of their treatment (Figure 3E).

Unresectable pancreatic tumors frequently cause obstructive jaundice, a highly morbid condition that can lead to biliary sepsis and death (3). Obstructive jaundice indicates local progression of the primary pancreatic tumor and is easily observed, as in Figure 3E. Jaundice was present in 29% (10/35) of mice who did not receive RT and was completely ameliorated in mice that received RT, with or without FG-4592 (0/29, Figure 3F; $P=0.02$).

EGLN Inhibition May Improve Survival by Ameliorating Radiation Toxicity

Although targeted, high-dose radiation reduced morbidity and subsequent death from local tumor progression, the median survival was most improved when RT was paired with FG-4592. An analysis of all-cause mortality demonstrated that local progression was the chief cause of death in 75% (21/28) of mice that received vehicle (Figure 4A) and 55% (6/11) of mice that received FG-4592 alone (Figure 4B). In comparison, 56% (5/9) of mice that received high-dose RT without radioprotection died from GI bleeding (Figure 4C). No gastrointestinal bleeding was observed in mice that received therapeutic ablative doses of RT with FG-4592 (Figure 4D; $P<.0001$), as these mice died chiefly from disease outside the radiation field.

Morbid gastrointestinal bleeding caused mice to become moribund, leading to euthanasia. An example of such extensive bleeding from a VEH + RT mouse is shown in Figure 4E. Histopathologic analyses from VEH + RT mice with gastrointestinal bleeding (Figure 4F) revealed patches of multifocal necrosis of epithelium lining crypts and villi, and expansion of the lamina propria by leukocytic infiltration, edema, congestion, and hemorrhage, consistent with the macroscopic pathology. Mice that received RT + FG-4592, however showed surprisingly little pathology other than edema and focal crypt necrosis with expansion of the adjacent lamina propria by leukocytic infiltration (Figure 4G).

FG-4592 maintains intestinal function during ablative radiotherapy

Although gastrointestinal bleeding was the most common morbid radiation injury in our model, generalized intestinal dysfunction in the form of diarrhea or fluid malabsorption could have also contributed to morbidity leading to euthansia. To quantify these changes in physiology, we performed a metabolic cage analysis of mice undergoing RT, with either FG-4592 or vehicle control for radioprotection. Metabolic cages enable the quantification of daily food and water consumption, as well as urine and fecal output. A decrease in formed fecal pellets indicate diarrhea, since they would be liquid and could not be collected in the

metabolic chamber (11). We found that mice treated with FG-4592 throughout radiation had more formed feces compared to vehicle controls (Figure 5A and quantified in Figure 5B), without any differences in food intake (Figure S4A and quantified in S4B). This increase in formed stools indicates less diarrhea in mice receiving FG-4592. Similarly, FG-4592 increased both urine output (Figure 5C and quantified in Figure 5D) and water consumption (Figure S4C and quantified in S4D), which indicate that FG-4592 promoted the maintenance of absorptive functions of the GI tract during ablative RT.

EGLN inhibition reduces apoptosis and increases microvessel density after RT

To better understand how EGLN inhibition reduces gastrointestinal toxicity, we subjected C57BL/6 mice to 15 fractions of upper abdominal RT (as in Figure 1B) with FG-4592 (FG +RT) or vehicle controls (VEH + RT) along with unirradiated mice given only vehicle by oral gavage (VEH, see scheme in Figure 6A). Mice were sacrificed 5 days after the last fraction (30) and the small intestines from the proximal duodenum through the 2nd portion of the jejunum were collected and processed so that the entire GI tract could be analyzed as a single longitudinal section (see examples in Figure S5, (20)). We found that radiated mice protected with FG-4592 had intestines that were morphologically indistinguishable from unirradiated controls (Figure 6B and Figure S5). On the other hand, 40% of VEH +RT animals (2/5) showed patches of villi blunting and crypt hypertrophy in the duodenum (Figure 6B and Figure S5, middle panel), consistent with known mechanisms of radiation injury to the gastrointestinal tract.

We then quantified epithelial apoptosis with terminal deoxynucleotidyl transferase–mediated deoxyuridine triphosphate nick end labeling (TUNEL) staining in these intestines. Mice that received radiation had significantly more apoptosis in their intestines than unirradiated controls (Figure 6C and examples in 6D). The addition of FG-4592 reduced TUNEL+ foci in epithelial cells by two fold compared to VEH + RT controls indicating a protective effect.

EGLN inhibition has been also shown to enhance local production of vascular endothelial growth factor (VEGF) in a HIF-dependent manner, which may partially mediate some of its radioprotective effects (11). Indeed, we measured microvessel density (MVD) in each of the three cohorts and found that MVD was increased by 80% in the mice treated with FG-4592 (Figure 6E with examples in 6F). These increases in MVD were correlated with a 74% increase in *Vegf* mRNA expression in intestinal epithelial cells, as determined by qPCR (Figure 6G).

Discussion

Our preclinical data illustrates why it is feasible and desirable to treat locally advanced pancreatic tumors with ablative radiation (Figure 6H). Without appropriate localized therapy, mice die from local progression (Figure 3G and 4A), which mimics what sometimes occurs in patients with unresectable pancreatic cancer (3). The addition of ablative radiation reduces deaths from local disease, but also causes unacceptable treatment toxicity without radioprotection, which reflects a common barrier to curative treatment in unresectable pancreatic cancer (9). The use of the radioprotective EGLN inhibitor FG-4592, however,

eliminated intestinal dysfunction and gastrointestinal bleeding and enabled higher radiation doses to pancreatic tumors without tumor protection.

There are several mechanistic considerations for radiation protection by FG-4592. The bulk of our mechanistic understanding of radiation injury and protection comes from models of radiation-induced gastrointestinal syndrome (RIGS), which use a single fraction of high-dose radiation to the whole body, or at least the entire abdomen. In this context, EGLN inhibition has been shown by three different groups to increase survival (12), improve gastrointestinal function (11), and reduce apoptosis (13) compared to unprotected controls. In this study, we demonstrate that EGLN inhibition in the form of oral FG-4592 also has similar protective effect, improving survival and reducing diarrhea after high-dose fractionated radiation to a limited field. This is a critical finding, since treatments for RIGS may not protect the gut from fractionated radiation (31), since these timecourse and nature of radiation injury and subsequent recovery are quite different.

Another critical finding in our study is that FG-4592 eliminates radiation-induced gastrointestinal bleeding, which is a highly morbid complication that arises during pancreatic radiation. The exact mechanism of how FG-4592 reduces gastrointestinal bleeding is still under active investigation, but it may be related to local Vegf production in the intestines which may increase microvessel density (Figure 6E and 6G). To our knowledge, FG-4592 is the only drug that is able to protect the intestines from the most concerning gastrointestinal side effects of radiation: diarrhea and gastrointestinal bleeding.

A common concern with radioprotectors is that they may inadvertedly shield tumors from cytotoxic therapy. Our data clearly demonstrate that EGLN inhibition selectively protects normal tissues because FG-4592 stabilizes HIF in normoxic tissues like the intestines (Figure 1A), but does not further enhance HIF levels in hypoxic tissues, like pancreatic tumors ((26), Figure 2A). Importantly, EGLN inhibition and subsequent downstream HIF activation does not stimulate tumor growth in our model. Direct HIF2 expression in a KPC orthotopic model slowed tumor growth and improved survival, which is consistent with recent publications that also suggested that both HIF1 and HIF2 have tumor suppressive roles in tissue specific contexts. For instance, in preclinical models of lung cancer (32), and pancreatic cancer (33), HIF deletion enhanced tumor growth, whereas direct overexpression of HIF2 in a sarcoma model (27) suppressed tumor progression. We were surprised to find that systemic EGLN inhibition directly improved survival compared to vehicle controls (Figure 3C). These unexpected tumor suppressive effects of systemic FG-4592 are likely mediated by a cell-autonomous mechanism, since the drug did not alter HIF expression in tumors (Figure 2A). This possibility is supported by previous studies where EGLN inhibition reshaped the tumor microenviroment to be more responsive to treatment (34).

There are several limitations to this study. The first is that chemotherapy was not administered in our experimental model. Neaoadjuvant chemotherapy such as gemcitabine/nab-paclitaxel (35) or FOLFIRINOX (36) is considered the standard of care in nearly all stages of pancreatic cancer. Patients with locally advanced pancreatic cancer are typically given chemotherapy for many months and restaged several times. Patients whose primary pancreatic tumor remain stable without evidence of metastatic progression can then be

considered for consolidative ablative radiotherapy (2). In the present study, mice were not staged beyond focused pancreatic ultrasounds, and it is possible mice with pre-existing metastatic disease or harbored other unfavorable features that would not have been detected by ultrasound alone. Indeed, only 17 of the 31 mice that received RT were able to receive a full dose (Table S1 and S2). Mice that did not receive a full dose died of rapid disease progression that likely existed at the time of enrollment (Figure 4, Table S1 and S2). These outcomes reinforce the notion that optimal chemotherapy should be administered first to control metastatic disease before offerering intensive local treatment, such as ablative RT. Future preclinical and clinical efforts in unresectable pancreatic cancer must incorporate modern chemotherapy regimens (35–37) to further improve survival gains by better controlling metastatic microscopic disease.

Another limitation is that there is currently no biomarker to determine which patients are ideal for consolidation with radiation and who might benefit from EGLN inhibitors. For the former, there is continuing work on histologic biomarkers such as SMAD4 (38) as well as circulating tumor DNA(39), and radiomic (40,41) approaches. For the latter issue, there is no clinically accepted biomarker for hypoxia. Although we posit that HIF expression is high in pancreatic tumors and low in normal tissues as has been observed in resected pancreatic cancer (42), it is unclear if this concept can be extrapolated to locally advanced disease. This issue could be addressed with hypoxia imaging of tumors (43) in the setting of a clinical trial.

In other disease sites such as lung cancer (44) and liver cancer (45), high doses of focused radiation are used to approximate surgery when an operation is not possible. We envision that the use of radioprotectors like FG-4592 would enable ablative doses of radiotherapy to unresectable pancreatic cancer after receiving appropropriate induction chemotherapy. FG-4592 has a superior side effect profile compared to the only other FDA-approved radioprotector, intravenous amifostine, which causes significant hypotension and nausea (46) and could gain rapid acceptance in the clinic. Thus, an approach of ablative radiation enabled by EGLN inhibition could serve as a surrogate for surgery in patients with unresectable pancreatic cancer who respond to induction chemotherapy.

Supplementary Material

Refer to Web version on PubMed Central for supplementary material.

Acknowledgments:

We would like to acknowledge Ronald DePinho and Haoqiang Yang for their generous gift of KPC breeders for our colony. We thank Robert Bast and Joe Herman for their critical review of the data and manuscript.

Grant Support: C.M.T. was supported by funding from the Cancer Prevention & Research Institute of Texas (CPRIT) grant RR140012, V Foundation (V2015–22), Sidney Kimmel Foundation, Sabin Family Foundation Fellowship, and the McNair Family Foundation. Additional funding sources that supported this work include National Cancer Institute of the National Institutes of Health under award number R01CA207236 (to HPW). Support to MCB came from T32CA186892 and F31CA210631This work was also supported by the NIH/NCI under award number P30CA016672 for use of the Small Animal Imaging Facility.

References

1. Rahib L, Smith BD, Aizenberg R, Rosenzweig AB, Fleshman JM, Matrisian LM. Projecting cancer incidence and deaths to 2030: the unexpected burden of thyroid, liver, and pancreas cancers in the United States. Cancer Res 2014;74:2913–21 [PubMed: 24840647]
2. Balaban EP, Mangu PB, Khorana AA, Shah MA, Mukherjee S, Crane CH, et al. Locally Advanced, Unresectable Pancreatic Cancer: American Society of Clinical Oncology Clinical Practice Guideline. J Clin Oncol 2016;34:2654–68 [PubMed: 27247216]
3. Iacobuzio-Donahue CA, Fu B, Yachida S, Luo M, Abe H, Henderson CM, et al. DPC4 gene status of the primary carcinoma correlates with patterns of failure in patients with pancreatic cancer. J Clin Oncol 2009;27:1806–13 [PubMed: 19273710]
4. Kelly P, Das P, Pinnix CC, Beddar S, Briere T, Pham M, et al. Duodenal toxicity after fractionated chemoradiation for unresectable pancreatic cancer. International journal of radiation oncology, biology, physics 2013;85:e143–9
5. Krishnan S, Chadha AS, Suh Y, Chen HC, Rao A, Das P, et al. Focal Radiation Therapy Dose Escalation Improves Overall Survival in Locally Advanced Pancreatic Cancer Patients Receiving Induction Chemotherapy and Consolidative Chemoradiation. Int J Radiat Oncol Biol Phys 2016;94:755–65 [PubMed: 26972648]
6. Kim SK, Wu CC, Horowitz DP. Stereotactic body radiotherapy for the pancreas: a critical review for the medical oncologist. J Gastrointest Oncol 2016;7:479–86 [PubMed: 27284482]
7. Yan KS, Chia LA, Li X, Ootani A, Su J, Lee JY, et al. The intestinal stem cell markers Bmi1 and Lgr5 identify two functionally distinct populations. Proc Natl Acad Sci U S A 2012;109:466–71 [PubMed: 22190486]
8. Murphy JD, Christman-Skieller C, Kim J, Dieterich S, Chang DT, Koong AC. A dosimetric model of duodenal toxicity after stereotactic body radiotherapy for pancreatic cancer. Int J Radiat Oncol Biol Phys 2010;78:1420–6 [PubMed: 20399033]
9. Hoyer M, Roed H, Sengelov L, Traberg A, Ohlhuis L, Pedersen J, et al. Phase-II study on stereotactic radiotherapy of locally advanced pancreatic carcinoma. Radiother Oncol 2005;76:48–53 [PubMed: 15990186]
10. Kaelin WG Jr., Ratcliffe PJ. Oxygen sensing by metazoans: the central role of the HIF hydroxylase pathway. Mol Cell 2008;30:393–402 [PubMed: 18498744]
11. Taniguchi CM, Miao YR, Diep AN, Wu C, Rankin EB, Atwood TF, et al. PHD inhibition mitigates and protects against radiation-induced gastrointestinal toxicity via HIF2. Sci Transl Med 2014;6:236ra64
12. Ayrapetov MK, Xu C, Sun Y, Zhu K, Parmar K, D'Andrea AD, et al. Activation of Hif1alpha by the prolylhydroxylase inhibitor dimethyoxalyglycine decreases radiosensitivity. PLoS One 2011;6:e26064 [PubMed: 22016813]
13. Jalili-Firoozinezhad S, Prantil-Baun R, Jiang A, Potla R, Mammoto T, Weaver JC, et al. Modeling radiation injury-induced cell death and countermeasure drug responses in a human Gut-on-a-Chip. Cell Death Dis 2018;9:223 [PubMed: 29445080]
14. Tegley CM, Viswanadhan VN, Biswas K, Frohn MJ, Peterkin TA, Chang C, et al. Discovery of novel hydroxy-thiazoles as HIF-alpha prolyl hydroxylase inhibitors: SAR, synthesis, and modeling evaluation. Bioorg Med Chem Lett 2008;18:3925–8 [PubMed: 18579373]
15. Provenzano R, Besarab A, Wright S, Dua S, Zeig S, Nguyen P, et al. Roxadustat (FG-4592) Versus Epoetin Alfa for Anemia in Patients Receiving Maintenance Hemodialysis: A Phase 2, Randomized, 6- to 19-Week, Open-Label, Active-Comparator, Dose-Ranging, Safety and Exploratory Efficacy Study. Am J Kidney Dis 2016;67:912–24 [PubMed: 26846333]
16. Del Vecchio L, Locatelli F. Roxadustat in the treatment of anaemia in chronic kidney disease. Expert Opin Investig Drugs 2018;27:125–33
17. Bardeesy N, Aguirre AJ, Chu GC, Cheng KH, Lopez LV, Hezel AF, et al. Both p16(Ink4a) and the p19(Arf)-p53 pathway constrain progression of pancreatic adenocarcinoma in the mouse. Proc Natl Acad Sci U S A 2006;103:5947–52 [PubMed: 16585505]
18. Tran TT, Gupta N, Goh T, Naigamwalla D, Chia MC, Koohestani N, et al. Direct measure of insulin sensitivity with the hyperinsulinemic-euglycemic clamp and surrogate measures of insulin

sensitivity with the oral glucose tolerance test: correlations with aberrant crypt foci promotion in rats. Cancer Epidemiol Biomarkers Prev 2003;12:47–56 [PubMed: 12540503]

19. Hu CJ, Wang LY, Chodosh LA, Keith B, Simon MC. Differential roles of hypoxia-inducible factor 1alpha (HIF-1alpha) and HIF-2alpha in hypoxic gene regulation. Mol Cell Biol 2003;23:9361–74 [PubMed: 14645546]
20. Tinkum KL, Stemler KM, White LS, Loza AJ, Jeter-Jones S, Michalski BM, et al. Fasting protects mice from lethal DNA damage by promoting small intestinal epithelial stem cell survival. Proc Natl Acad Sci U S A 2015;112:E7148–54 [PubMed: 26644583]
21. Kirsch DG, Santiago PM, di Tomaso E, Sullivan JM, Hou WS, Dayton T, et al. p53 controls radiation-induced gastrointestinal syndrome in mice independent of apoptosis. Science 2010;327:593–6 [PubMed: 20019247]
22. Seifert L, Werba G, Tiwari S, Giao Ly NN, Nguy S, Alothman S, et al. Radiation Therapy Induces Macrophages to Suppress T-Cell Responses Against Pancreatic Tumors in Mice. Gastroenterology 2016;150:1659–72 e5 [PubMed: 26946344]
23. Qiu W, Carson-Walter EB, Liu H, Epperly M, Greenberger JS, Zambetti GP, et al. PUMA regulates intestinal progenitor cell radiosensitivity and gastrointestinal syndrome. Cell Stem Cell 2008;2:576–83 [PubMed: 18522850]
24. Tuli R, Surmak A, Reyes J, Hacker-Prietz A, Armour M, Leubner A, et al. Development of a novel preclinical pancreatic cancer research model: bioluminescence image-guided focal irradiation and tumor monitoring of orthotopic xenografts. Transl Oncol 2012;5:77–84 [PubMed: 22496923]
25. Ying H, Kimmelman AC, Lyssiotis CA, Hua S, Chu GC, Fletcher-Sananikone E, et al. Oncogenic Kras maintains pancreatic tumors through regulation of anabolic glucose metabolism. Cell 2012;149:656–70 [PubMed: 22541435]
26. Koong AC, Mehta VK, Le QT, Fisher GA, Terris DJ, Brown JM, et al. Pancreatic tumors show high levels of hypoxia. Int J Radiat Oncol Biol Phys 2000;48:919–22 [PubMed: 11072146]
27. Nakazawa MS, Eisinger-Mathason TS, Sadri N, Ochocki JD, Gade TP, Amin RK, et al. Epigenetic re-expression of HIF-2alpha suppresses soft tissue sarcoma growth. Nat Commun 2016;7:10539 [PubMed: 26837714]
28. Haston CK. Mouse genetic approaches applied to the normal tissue radiation response. Front Oncol 2012;2:94 [PubMed: 22891164]
29. Morton JP, Timpson P, Karim SA, Ridgway RA, Athineos D, Doyle B, et al. Mutant p53 drives metastasis and overcomes growth arrest/senescence in pancreatic cancer. Proc Natl Acad Sci U S A 2010;107:246–51 [PubMed: 20018721]
30. Tucker SL, Thames HD, Brown BW, Mason KA, Hunter NR, Withers HR. Direct analyses of in vivo colony survival after single and fractionated doses of radiation. Int J Radiat Biol 1991;59:777–95 [PubMed: 1672365]
31. Lee CL, Oh P, Xu E, Ma Y, Kim Y, Daniel AR, et al. Blocking cyclin-dependent kinase 4/6 during single dose vs. fractionated radiation therapy leads to opposite effects on acute gastrointestinal toxicity in mice. Int J Radiat Oncol Biol Phys 2018
32. Mazumdar J, Hickey MM, Pant DK, Durham AC, Sweet-Cordero A, Vachani A, et al. HIF-2alpha deletion promotes Kras-driven lung tumor development. Proc Natl Acad Sci U S A 2010;107:14182–7 [PubMed: 20660313]
33. Lee KE, Spata M, Bayne LJ, Buza EL, Durham AC, Allman D, et al. Hif1a Deletion Reveals Pro-Neoplastic Function of B Cells in Pancreatic Neoplasia. Cancer Discov 2016;6:256–69 [PubMed: 26715642]
34. Mazzone M, Dettori D, Leite de Oliveira R, Loges S, Schmidt T, Jonckx B, et al. Heterozygous deficiency of PHD2 restores tumor oxygenation and inhibits metastasis via endothelial normalization. Cell 2009;136:839–51 [PubMed: 19217150]
35. Von Hoff DD, Ervin T, Arena FP, Chiorean EG, Infante J, Moore M, et al. Increased survival in pancreatic cancer with nab-paclitaxel plus gemcitabine. N Engl J Med 2013;369:1691–703 [PubMed: 24131140]
36. Conroy T, Desseigne F, Ychou M, Bouche O, Guimbaud R, Becouarn Y, et al. FOLFIRINOX versus gemcitabine for metastatic pancreatic cancer. N Engl J Med 2011;364:1817–25 [PubMed: 21561347]

37. Vaccaro V, Sperduti I, Milella M. FOLFIRINOX versus gemcitabine for metastatic pancreatic cancer. N Engl J Med 2011;365:768–9; author reply 9 [PubMed: 21864184]

38. Taniguchi C, Maitra A. It's a SMAD/SMAD World. Cell 2015;161:1245–6 [PubMed: 26046433]

39. Bernard V, Kim DU, San Lucas FA, Castillo J, Allenson K, Mulu FC, et al. Circulating Nucleic Acids Associate with Outcomes of Patients with Pancreatic Cancer. Gastroenterology 2018

40. Koay EJ, Amer AM, Baio FE, Ondari AO, Fleming JB. Toward stratification of patients with pancreatic cancer: Past lessons from traditional approaches and future applications with physical biomarkers. Cancer Lett 2016;381:237–43 [PubMed: 26806807]

41. Amer AM, Zaid M, Chaudhury B, Elganainy D, Lee Y, Wilke CT, et al. Imaging-based biomarkers: Changes in the tumor interface of pancreatic ductal adenocarcinoma on computed tomography scans indicate response to cytotoxic therapy. Cancer 2018;124:1701–9 [PubMed: 29370450]

42. Colbert LE, Fisher SB, Balci S, Saka B, Chen Z, Kim S, et al. High nuclear hypoxia-inducible factor 1 alpha expression is a predictor of distant recurrence in patients with resected pancreatic adenocarcinoma. Int J Radiat Oncol Biol Phys 2015;91:631–9 [PubMed: 25596110]

43. Taylor E, Yeung I, Keller H, Wouters BG, Milosevic M, Hedley DW, et al. Quantifying hypoxia in human cancers using static PET imaging. Phys Med Biol 2016;61:7957–74 [PubMed: 27779123]

44. Timmerman RD, Paulus R, Pass HI, Gore EM, Edelman MJ, Galvin J, et al. Stereotactic Body Radiation Therapy for Operable Early-Stage Lung Cancer: Findings From the NRG Oncology RTOG 0618 Trial. JAMA Oncol 2018

45. Hong TS, Wo JY, Yeap BY, Ben-Josef E, McDonnell EI, Blaszkowsky LS, et al. Multi-Institutional Phase II Study of High-Dose Hypofractionated Proton Beam Therapy in Patients With Localized, Unresectable Hepatocellular Carcinoma and Intrahepatic Cholangiocarcinoma. J Clin Oncol 2016;34:460–8 [PubMed: 26668346]

46. Hospers GA, Eisenhauer EA, de Vries EG. The sulfhydryl containing compounds WR-2721 and glutathione as radio- and chemoprotective agents. A review, indications for use and prospects. British journal of cancer 1999;80:629–38 [PubMed: 10360638]

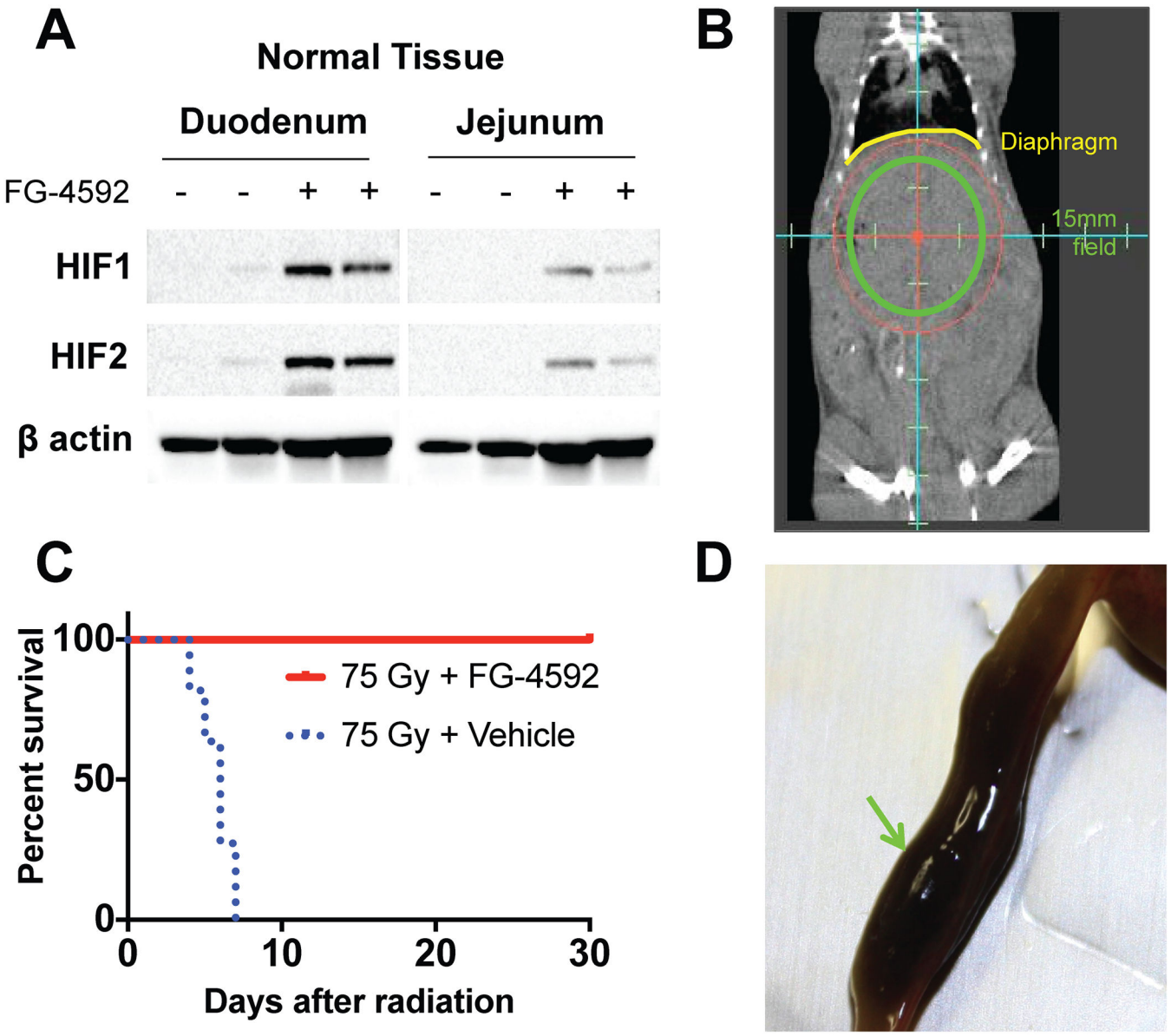

Figure 1. FG-4592 reduces morbidity from high-dose fractionated radiation

(**A**) Western blots demonstrating stabilized HIF in the duodenum and jejunum 6 hours after receiving FG-4592, representative of 4 mice per treatment condition. (**B**) Coronal image from a cone-beam CT taken during treatment with the circular 15mm field superimposed. Diaphragm (yellow) is pointed out for reference. (**C**) Improved survival of mice treated with FG-4592 after 75Gy/15fx of UA-XRT (n=8–10/tx cohort, Log rank p<0.0001). (**D**) Example of a duodenum lumen filled with partially digested blood (green arrow) as a result of radiation toxicity.

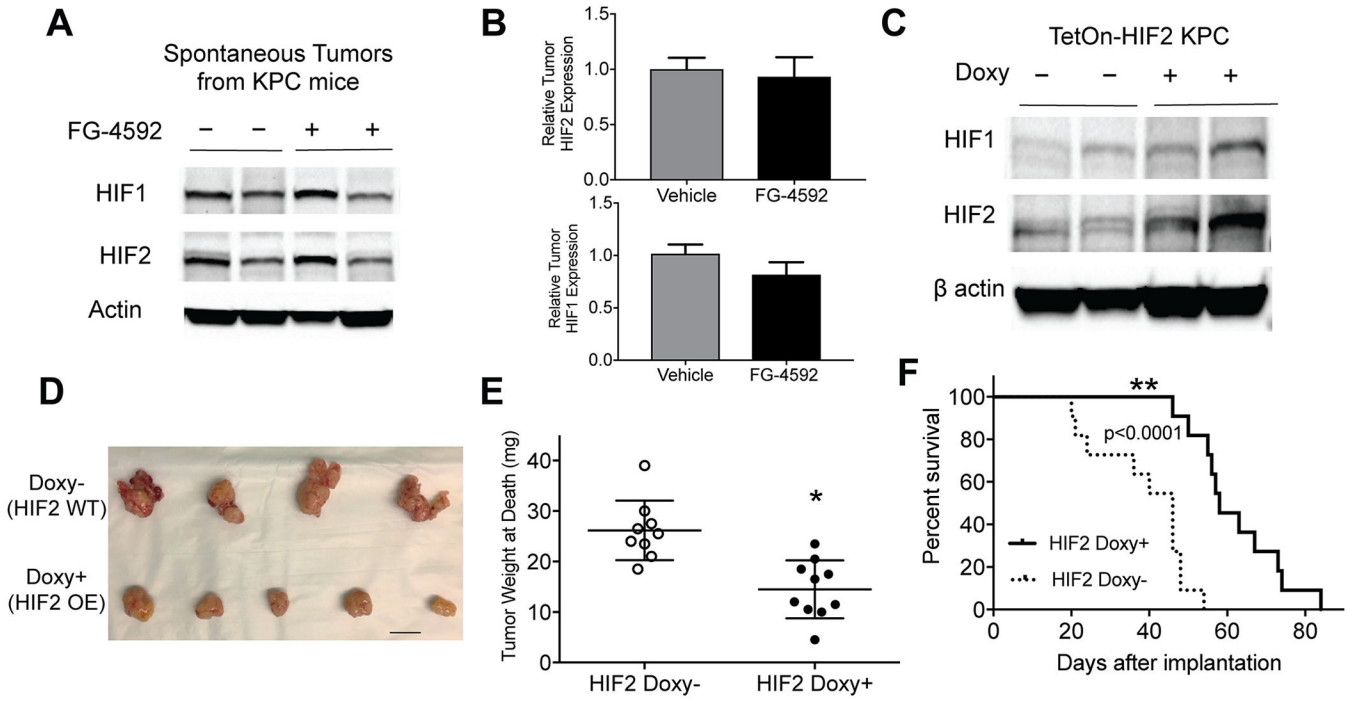

Figure 2. HIF stabilization within KPC tumors does not enhance tumor growth.

(**A**) EGLN inhibition by FG-4592 does not increase HIF expression by Western Blot, representative of 4–6 tumors per treatment group, with quantified relative levels of HIF1 and HIF2 in (**B**, error bars represent s.e.m.). (**C**) Overexpression of HIF2 in syngeneic orthotopic KPC tumors confirmed by Western Blot which are representative of 4 tumors from each treatment group. HIF2 expression decreased tumor growth as determined by visual inspection (**D**, scale bar=10mm) and tumor weight (**E**, n=9–10/cohort; unpaired two-tailed t-test **P*=0.0004, error bars are s.e.m.), contributing to improved survival (**F**, n=11 per cohort, log rank *P*<0.0001)

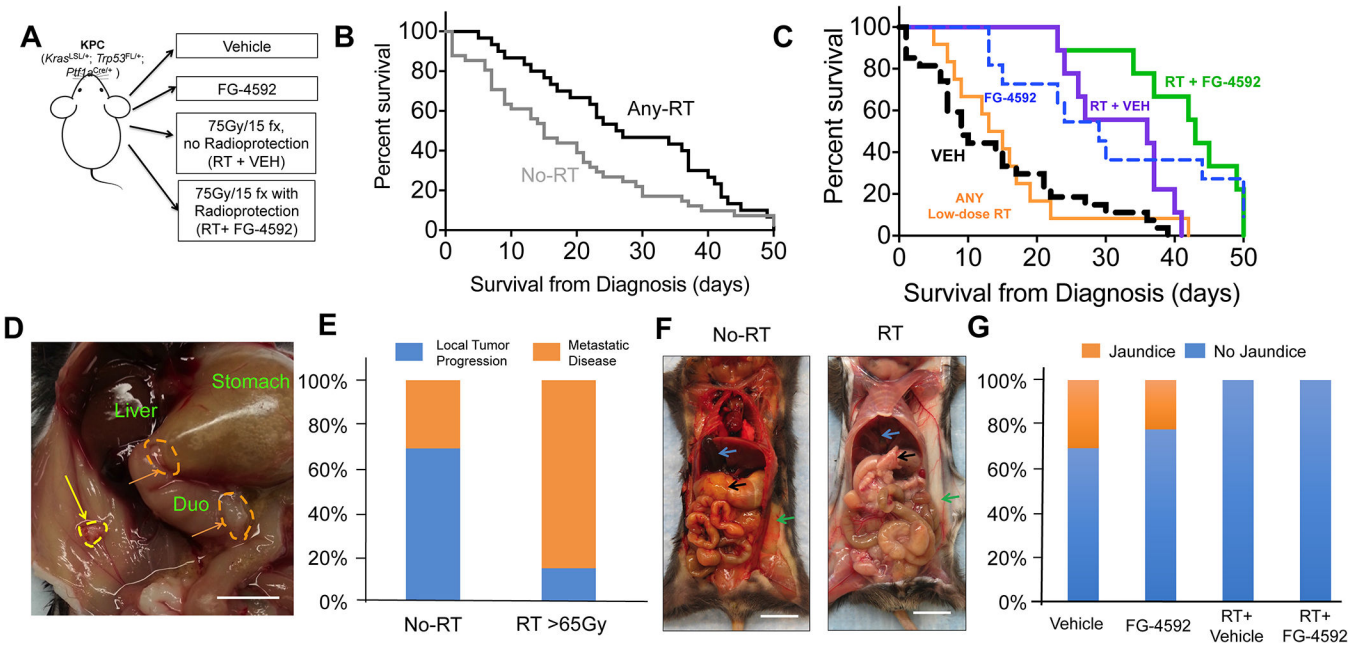

Figure 3. High-dose radiation with concurrent FG-4592 improves survival and reduces clinical signs of local progression

(**A**) Experimental scheme for KPC animals. (**B**) Kaplan-Meier survival curves for mice who received any radiation (any-RT= RT+VEH or RT+FG) or no radiation therapy (No-RT=VEH or FG) as part of their therapy. Median survival was higher in Any-RT group compared to No-RT (Gehan-Breslow-Wilcoxan P=0.006). **(C)** Kaplan-Meier survival curves for all animals, with highest overall survival for mice treated with RT + FG-4592 (Log rank P<. 0001). (**D**) Gross photograph of the abdominal cavity of a mouse with local tumor dissemination. The wall of the gastric antrum (orange dashed line) and duodenum is thickened by invading cancer cells, which have obstructed gastric outflow leading to gastric bloating. There is a single tumor nodule (yellow arrow) in the peritoneal wall. Scale bar=5mm (**E**) Local tumor progression more commonly necessitated euthanasia in No-RT treatment groups compared to those that received >65Gy radiation treatment (Fisher's exact P<0.001) (**F**) An illustrative example of jaundice. Icteric KPC mouse that had no RT (left image) and an non-icteric KPC mouse treated with RT (right image). The pancreas (black arrow), subcutaneous fat (green arrow) and the gallbladder (blue arrow) are shown in both mice. Scale bar=1cm (**G**) Mice who did not receive RT had higher rates of jaundice (Chi-square P=0.02)

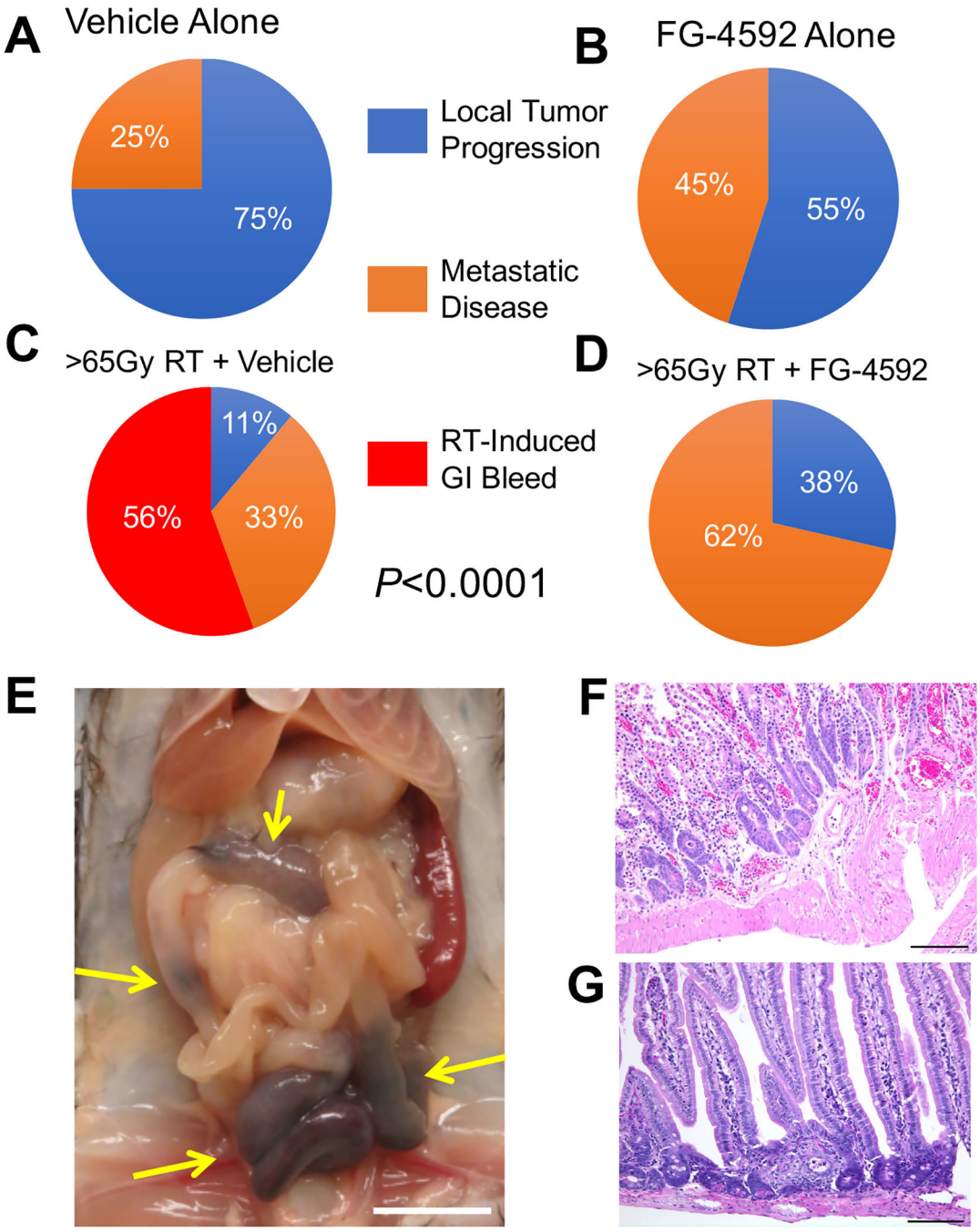

Figure 4. EGLN inhibition by FG-4592 reduces toxicity and enables definitive radiation treatment of pancreatic cancer.

Distribution of all causes of morbidity leading to death for (**A**) Vehicle alone, (**B**) FG-4592 alone, (**C**) >65Gy RT + Vehicle and (**D**) >65Gy RT + FG-4592. (**E**) An example of intestinal bleeding (arrows) observed at necropsy in a mouse that received 75Gy of fractionated radiation without radioprotection (scale bar=1cm) with (**F**) histopathologic correlation from the same mouse showing edema, hemorrhage, and leukocytic infiltration. (**G**) Representative histopathology of a jejunal section at necropsy from mouse treated with full dose ablative

RT with FG-4592 for radioprotection. The major lesions identified were edema, focal crypt necrosis, and leukocytic infiltration.

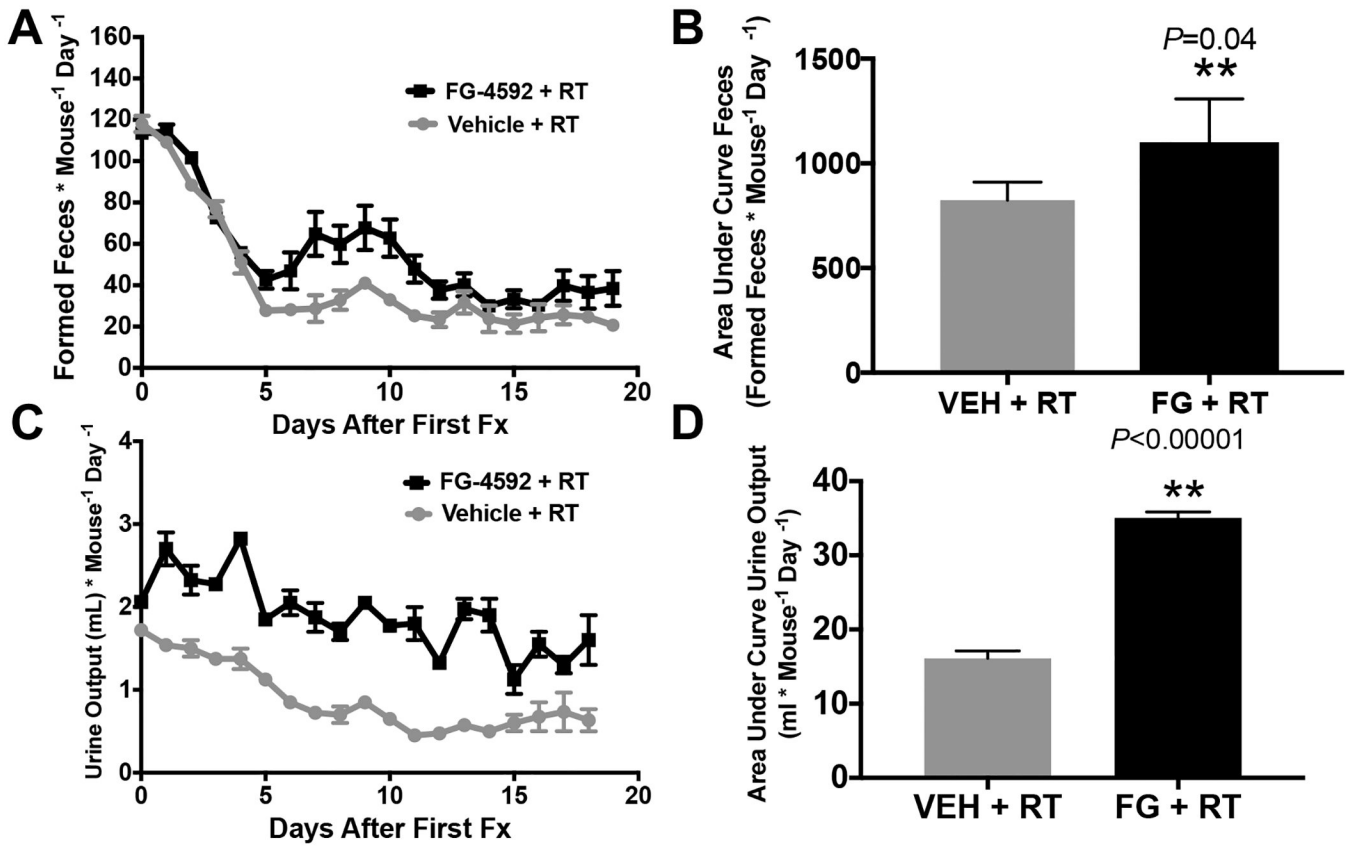

Figure 5. Metabolic cage analysis of mice treated with a clinically relevant course of dose-escalated RT to a limited upper abdominal field.

(A) Formed feces during fractionated radiation treatments with area under the curve quantification in (B). More formed feces denotes less diarrhea, as loose stools cannot be quantified in metabolic cage method. (C) Urine output during fractionated radiation treatments with area under the curve quantification in (D).

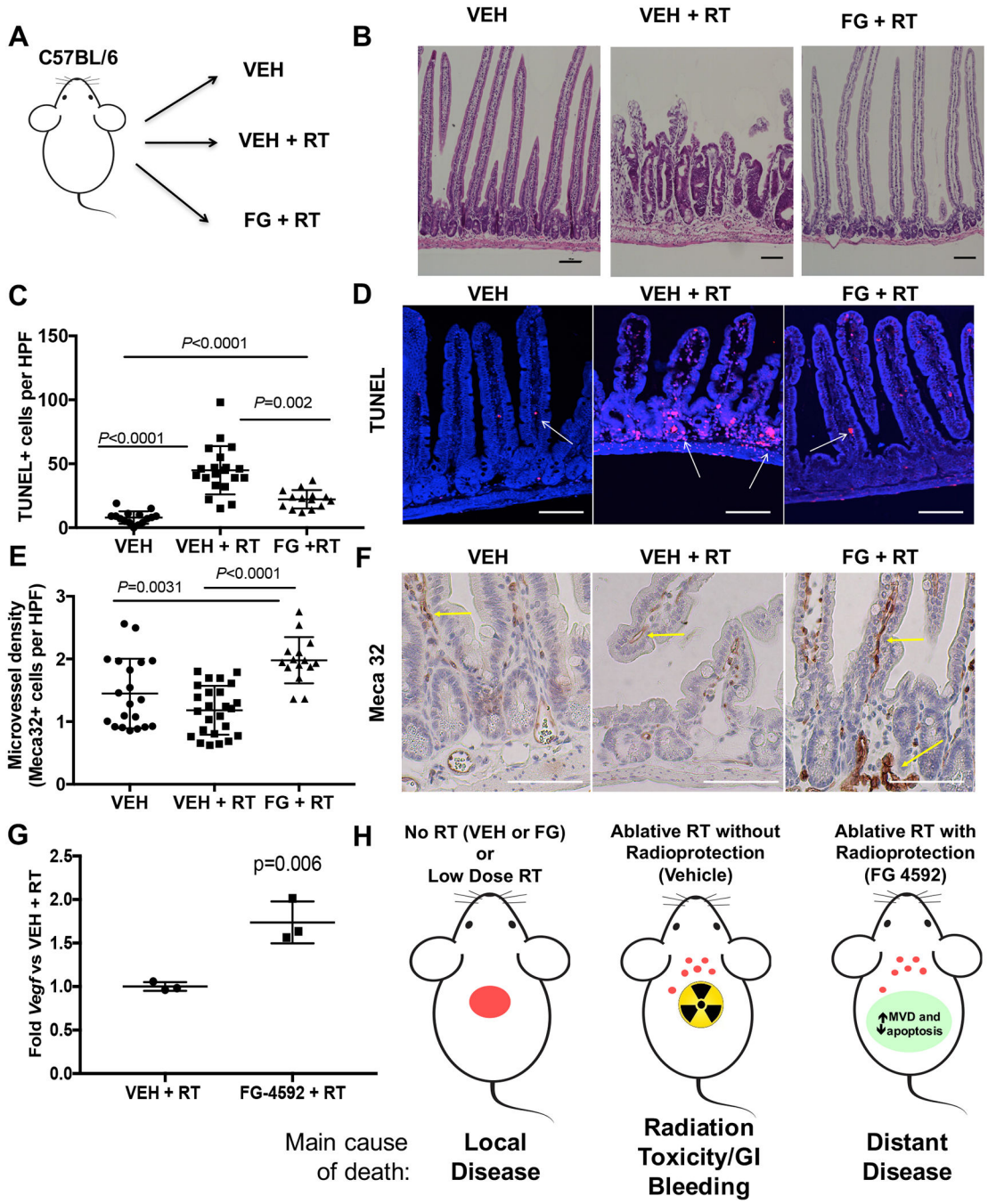

Figure 6. Mechanisms of FG-4592 Intestinal radioprotection.

(A) Scheme of experimental groups, where mice received daily vehicle alone (VEH), vehicle with 75Gy/15 fractions of radiation (VEH +RT) or FG-4592 with the same radiation treatment (FG +RT). Intestines from the proximal duodenum to the second portion of the jejunum were collected and analyzed over serial ongitudinal sections (see methods). (B) Representative images of lesions observed from H&E-stained small intestines of VEH (n=5), 75Gy/15 fractions (n=5), and 75Gy/15 fraction + FG-4592 treated mice (n=5) observed in the duodenum of RT+VEH group (2 of 5 animals), but not in other cohorts.

These lesions are characterized by villi blunting and crypt hypertrophy. Scale bars=100 μm (C) $TUNEL^+$ cells per HPF in the small intestines of the indicated groups with representative examples in (D). Scale bars=50 μm (E) Quantification of Meca-32 staining for endothelial cells in the epithelia of the small intestines within the three cohorts, quantified on 3–5 HPF per mouse, with representative images used for quantification in (F). Scale bars=50 μm. (G) Jejunal epithelium was isolated from each of the cohorts and assessed by quantitative PCR for relative mRNA levels of *Vegf*. (H) Schematic of rationale for radiation protection with high-dose radiation for unresectable pancreatic cancer. Radiation slows local progression, but often causes toxicity, but a combination of high-dose radiation along with FG-4592 for radioprotection provides local control while preventing toxicity from treatment, contributing to survival.